THE ASTROPHYSICAL JOURNAL, 464:498–506, 1996 June 10

YOHKOH OBSERVATIONS OF AN OVER-THE-LIMB SOLAR FLARE WITH LARGE SPECTRAL LINE SHIFTS

ALPHONSE C. STERLING[1]
Computational Physics Inc., 2750 Prosperity Avenue, Suite 600, Fairfax, VA 22031
LOUISE K. HARRA-MURNION
Mullard Space Science Laboratory, University College London, Holmbury St. Mary, Surrey RH5 6NT, UK
HUGH S. HUDSON
Institute for Astronomy, University of Hawaii, Honolulu, HI 96822
AND
JAMES R. LEMEN
Lockheed Solar and Astrophysics Laboratory, Department 91-30, B/252, 3251 Hanover Street, Palo Alto, CA 94304
Received 1995 September 11; accepted 1995 December 1

ABSTRACT

We present observations of a solar flare of 1993 April 15 near 9 UT, using data from the *Yohkoh* Bragg crystal spectrometer (BCS) and soft X-ray telescope (SXT). Observations from SXT indicate that the flare occurred well beyond the solar limb, meaning that our observations are restricted to the uppermost portions of the flaring structure. BCS spectra show strong bulk blueshifts of the spectral line profiles for a short period near the start of the event, followed by an extended period of strong bulk redshifts of the line profiles. Concurrent with these bulk line shifts, the spectra show "blue wing" asymmetries. Both bulk line shifts and blue wings are infrequent characteristics of flares observed near the solar limb. Our observations are consistent with strong upward mass motions occurring on a high-altitude flaring loop oriented edge-on with the Earth. We find nonthermal line broadenings in the spectra which are qualitatively and quantitatively similar to line broadenings in spectra of disk flares. Near peak intensity of the flare, $\lesssim 10\%$ of the residual nonthermal broadening can be explained by the spatial distribution of the soft X-ray flaring structure.

Subject headings: Sun: flares — Sun: X-rays, gamma rays

1. INTRODUCTION

Solar flares occurring at or near the solar limb can provide valuable information pertaining to the flaring mechanism. If these flares occur just beyond the solar limb, that is, with the lower portions of the flaring structure occulted by the solar limb, we are able to study the isolated upper portions of flares even with nonimaging solar instruments. Using this occultation method, Khan et al. (1995) and Mariska, Sakao, & Bentley (1996) have studied the spectral properties of the bright compact regions often seen near the tops of flaring loops in soft X-rays (Acton et al. 1992; Feldman et al. 1994; Doschek, Strong, & Tsuneta 1995), using the nonimaging Bragg crystal spectrometer (BCS) instrument on the *Yohkoh* satellite. In this paper we present *Yohkoh* observations of a flare which occurred beyond the solar limb on 1993 April 15, near 9:00 UT, and which had a soft X-ray classification of C1.2 as measured by the *Geostationary Operational Environmental Satellites* (*GOES*). This event displays unusually large spectral line shifts, consistent with Doppler shifts resulting from plasmas undergoing vigorous motions along the observing line of sight. Such Doppler shifts are uncommon in flares occurring at or near the limb (e.g., Doschek 1990), but they are occasionally seen. Fludra et al. (1989), for example, found substantial blueshifts in one out of eight limb flares they observed, and the work of Mariska (1994) also indicates line shifts in some limb events. Analysis of the 1993 April 15 event gives us insight into why strong line shifts are observed only infrequently in flares occurring near the solar limb, and also further information on the nature of plasma processes in the isolated upper portions of flares. We present observations from the Fe XXV, Ca XIX, and S XV channels of BCS, and we use data from the soft X-ray telescope (SXT), also on board *Yohkoh*, in our analysis. Fluxes recorded by the *Yohkoh* hard X-ray telescope are not sufficient for producing hard X-ray images of this event.

Line shifts in solar flare spectra can be classified roughly into two types: bulk line shifts and "blue wings." Bulk line shifts are characterized by shifts of the entire spectrum to shorter (blueshifts) or longer (redshifts) wavelengths, consistent with bulk plasma flows toward or away from Earth, respectively. According to numerical models of the often-quoted "evaporation model" of solar flares (e.g., Nagai & Emslie 1984; Mariska, Emslie, & Li 1989), bulk line shifts are expected when the initial coronal plasma is tenuous. In the evaporation model, strong upflows of strongly heated chromospheric material result from deposition of particles or thermal energy in the chromosphere. When the coronal density is not too high, the emission measure in the upward-moving plasma dominates the emission measure of the gas at rest. Bulk blue spectral line shifts were observed by *Yohkoh* in disk flares which occurred on 1991 November 9 (Doschek et al. 1992, 1994) and 1991 December 16 (Culhane et al. 1994). Similarly, bulk redshifted spectra would be produced by bulk motions of soft X-ray–emitting plasma moving away from Earth.

In contrast to bulk line shifts, blue wings appear as asymmetries on the short-wavelength side of spectral lines, being

[1] Current address: Institute for Space and Astronautical Science, Yoshinodai 3-1-1, Sagamihara, Kanagawa 229, Japan.

most easily detectable in the resonance lines ($1s^2\,{}^1S_0$–$1s2p\,{}^1P_1$ transition) for the ions observed by BCS. For many years, blue wings have been observed during the rise phase of solar flares occurring on the solar disk (see Doschek 1990, and references therein). They are often interpreted as resulting from the superposition of two distinct plasma populations: a population which is virtually at rest with respect to Earth and which generally contains the majority of the emission measure, and a second population moving toward the Earth generally containing a smaller amount of emission measure. (Recently, Newton, Emslie, & Mariska 1996 have extended this concept to a plasma population covering a continuum of velocities.) Emslie, Li, & Mariska (1992) show that blue wings without substantial bulk line shifts near flare onset result from numerical evaporation models of flares when the initial coronal density is high enough. "Red wings," that is, asymmetries on the long-wavelength side of spectral lines, if they exist, are difficult to discern in BCS spectra due to blending of the resonance lines with nearby satellite spectral lines.

In the next section we give a brief description of the instruments on board *Yohkoh* used in this study, and background information on the 1993 April 15 flare. In §§ 3 and 4, we present our observations from BCS and SXT, respectively, and we examine possible explanations and implications of our observations in § 5.

2. INSTRUMENTS AND DATA

Culhane et al. (1991) describe the *Yohkoh* BCS in detail, and Lang et al. (1992) discuss the instrument's in-flight performance. Briefly, spectral data from the *Yohkoh* BCS are from Bragg diffraction from four curved crystals covering spectral ranges that include the resonance lines and associated satellite lines of hydrogen-like iron, Fe XXVI (1.7636–1.8044 Å); helium-like iron, Fe XXV (1.8298–1.8942 Å); helium-like calcium, Ca XIX (3.1631–3.1912 Å); and helium-like sulfur, S XV (5.0160–5.1143 Å). These spectral ranges assume an on-axis flaring source. In practice, the actual wavelength ranges observed vary with the north-south location of the event, due to the orientation of the Bragg crystals with respect to the Sun (see Mariska 1994). X-rays refracted from the crystals are counted by two one-dimensional position sensitive proportional counters, with the two iron channels sharing one detector and the calcium and sulfur channels sharing the other detector. BCS is about an order of magnitude more sensitive than Bragg spectrometers flown on previous satellites. This allows for effective observations earlier in the development of flares than previously possible. A consequence of the high sensitivity, however, is that detector saturation occurs when intensity levels become large, exceeding *GOES* X-ray class of about M3.

Because of the north-south orientation of the crystal dispersions, a wavelength-position calibration is necessary to determine the absolute wavelengths. In addition to the possibility of Doppler shifts due to motions of the source toward or away from Earth, this implies that apparent line shifts can result if the X-ray–emitting source moves in the north-south direction on the solar disk over the duration of the flare being observed. There are two methods to resolve this ambiguity. One method results from the physical positioning of the two detectors. They are mounted on either side of the spacecraft oriented so that an offset to the south (north) of the X-ray source results in an apparent wavelength shift of the spectral lines to the blue (red) in the Ca-S detector, and an apparent wavelength shift to the red (blue) in the Fe-Fe detector. In contrast, line shifts produced by actual Doppler motions toward (away from) Earth result in wavelength shifts to the blue (red) in both detectors simultaneously. Therefore, inspecting near-simultaneous spectra from both detectors tells us whether the line shifts are caused by Doppler motions. A second method for resolving the ambiguity is to use soft X-ray images of the source from SXT, if available, to see whether observed BCS line shifts can be explained by movement of the source in the north-south direction. This second method assumes that BCS and SXT are observing the same source. We have found that both these methods indicate that the line shifts we find in the 1993 April 15 flare are almost entirely attributable to Doppler motions rather than to north-south movement of the source position.

For the present analysis, we use spectra from the Fe XXV, Ca XIX, and S XV channels, accumulated for 60 s. All spectra are corrected for dead-time effects in the position-encoding electronics. This effect is estimated from the ratio of the photons counted from the detector anode to the photons counted from the cathode readout. All spectra are also corrected for effects resulting from the curvature of the Bragg crystal and for sensitivity variations as a function of position on the crystal as determined from prelaunch measurements.

Tsuneta et al. (1991) describe in detail the characteristics of the *Yohkoh* SXT. In short, SXT is a grazing incidence soft X-ray telescope equipped with a set of five filters with differing bandpasses. These filters allow for coverage of the wavelength range extending from 3 to 45 Å. Images obtained with the Be filter, spanning 3–10 Å, cover the temperature range closest to that of the BCS. For this reason, we use primarily Be filter data for comparing SXT data with the BCS observations in this work. X-ray images are recorded onto a 1024 × 1024 CCD with a pixel size of 2.″455. In normal quiet-Sun observations, SXT reads out the entire CCD at "half" or "quarter" resolution, thereby obtaining full-frame images of the full solar disk with a 2 × 2 or 4 × 4 summation over pixels. During flares, the SXT reads out a 64 × 64 pixel subregion of the CCD at a time resolution of up to 2 s; this is the partial frame imaging mode of SXT. Partial frame SXT coverage of the 1993 April 15 event spans approximately 09:06–09:16 UT.

It is difficult to establish with certainty the location of occurrence of flares near the limb. We can estimate which active region the 1993 April 15 flare occurred in by inspecting a movie of composite full-frame SXT images beginning several days prior to the event. Figure 1 (Plate 15) shows two full-frame thin Al filter images from SXT, the left panel from 5 days before the flare and the right panel from during the time of the flare itself; the flare is the bright extension beyond the west limb indicated by the arrow. West is to the right and north is up in the images. These images are both taken from the standard SXT movie, which has been corrected for stray light, background, and saturation effects. NOAA identifies two of the active regions near the west limb in the left panel as AR 7469 (at S06, W53 on April 11 at 0 UT, indicated by the arrow) and AR 7465 (at S06, W79). These two regions are the only ones which appear to be possible sources for the April 15 flare.

By applying the differential rotation model of Howard, Harvey, & Forgach (1990) to region 7469 on 1993 April 11, we estimate that the region crossed the limb at 13.7 hours on

PLATE 15

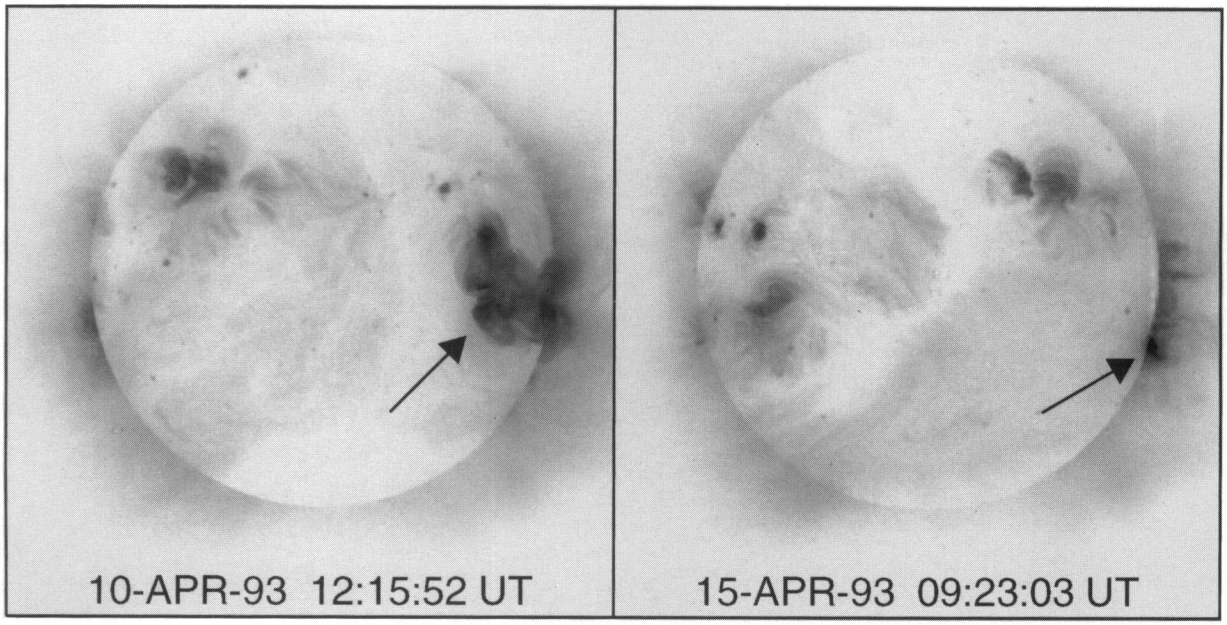

FIG. 1.—Composite full-frame SXT images from (*left*) several days before the 1993 April 15 flare and (*right*) the time of the flare, which appears on the west limb near latitude S19 (indicated by arrow). North is up and west is to the right in the images. Most likely, the active region indicated by the arrow inside the west limb of the April 10 image produced the flare after rotating to the far side of the Sun. Both images were obtained with the SXT thin Al filter. A coronal hole near the central meridian in the left panel has rotated off the disk by the time of the image in the right panel.

STERLING et al. (see 464, 499)

1993 April 13 and that the flare occurred with the region at longitude 114°. Similarly, extrapolating ground-based data from earlier dates, we estimate that region 7465 crossed the limb on April 11 at 18.2 hr and was near longitude 150° at the time of the flare's occurrence. Therefore, the flare occurred substantially on the far side of the Sun, and much of the lower portion of the flaring structure must have been occulted by the solar limb. This is fully consistent with the appearance of the SXT images as described later.

We can estimate the height of occultation of the flare-related structures, h, using

$$h \approx R_0[\sec(2\pi t/P) - 1], \quad (1)$$

where R_0 is the solar radius at the latitude of the active region, t is the time elapsed since limb transit, and P is the rotation period at the latitude of the active region. For NOAA 7469, the angles involved are small, so that equation (1) is $h \approx 37t^2$, with h in kilometers and t in hours. This gives an occultation height of 50–85,000 km, where the range comes from uncertainties in the location of the flare in the active region. Our calculation assumes that the flaring loops extend perpendicular to the solar surface. This is probably not the case, however, since the two active regions were centered near latitude S06 and the April 15 flare was near latitude S19. Inspection of SXT images from April 12 indicates that NOAA 7469 had structures extending from the bright core of the active region down to at least latitude S19. So if the flare did occur in that active region, then our estimate of the length of the occulted flaring loops may be too low by some 10,000 km. If the flare occurred in NOAA 7465, which was much further around the limb than NOAA 7469, then the amount of the flare occulted would be much greater, around 600,000 km. This would necessitate the existence of huge flaring structures, larger than we consider likely (Kane et al. 1992, however, did observe hard X-rays from a flare at longitude near 130°). Therefore, we assume that the source of the flare was active region NOAA 7469.

Our BCS observations start just after 9:00 UT and extend until just after 9:24 UT. Because of the southerly location of the flare, the resonance lines of Ca XIX and S XV are near the short-wavelength limit of the observation window, due to the north-south wavelength offset effect noted above. This effect is more pronounced in the S XV spectra, where virtually none of the continuum at wavelengths shorter than the resonance line is observable and any detectable blue wings to the resonance line during the rise phase would extend beyond the observed wavelength range. However, we are still able to observe the peak positions on the resonance lines in S XV (as well as in Ca XIX and Fe XXV) at all times for this event.

3. OBSERVATIONS FROM BCS

We derive electron temperature, fluxes (emission measures), nonthermal velocities, and line shift information from Fe XXV, Ca XIX, and S XV spectra for the 1993 April 15 flare.

In order to derive these parameters, we perform minimized χ^2 fits to the observed spectra using synthetic spectra. Temperature sensitivity comes primarily from ratios of resonance lines and dielectronic satellites for the various ions. For all three channels, our synthetic spectra assume isothermal plasmas and Voigt profiles for the line shapes. Lower stage ion fractions are from Arnaud & Raymond (1992) for Fe XXV and Arnaud & Rothenflug (1985) for Ca XIX and S XV. Atomic data are from Bely-Dubau et al. (1982a) for Fe XXV, from Bely-Dubau et al. (1982b) for Ca XIX, and from Harra-Murnion et al. (1996) for S XV. When fitting Fe XXV and Ca XIX spectra for early times in the development of the flare, we generally use a superposition of two separate spectra (i.e., two-component fits) in order to fit the spectral line profiles better when blue wings are present. We call the persistent spectral component the primary component and the transient blue wing component the secondary component. For the Fe XXV fits, we restricted some of the fit parameters before doing the minimized χ^2 analysis using parameters based on results from the free-parameter spectral fitting method discussed in Sterling, Doschek, & Pike (1994). Only single-component synthetic spectra are fitted to S XV spectra since, as noted in § 2, some of the S XV blue wing falls outside the channel observation window due to the southerly location of the flare. As is typical in Bragg observations of disk flare spectra, asymmetries in spectral lines due to blue wings disappear during the peak and decay phases of this event. Accordingly, at later times during the event we use only single-component spectral fits for all channels.

Figure 2 shows some results derived from BCS. Figure 2*a* gives fluxes for Fe XXV, Ca XIX, and S XV as functions of time (where the S XV values are reduced by a factor of 3). Figure 2*b* shows the electron temperatures, T_e, for the three channels, Figure 2*c* plots the nonthermal velocity, v_{nt}, for the three channels as functions of time. In each panel, thick solid, thin solid, and dashed lines represent Ca XIX, Fe XXV, and S XV quantities, respectively. When two-component fits are used at early times, we show only v_{nt} for the primary

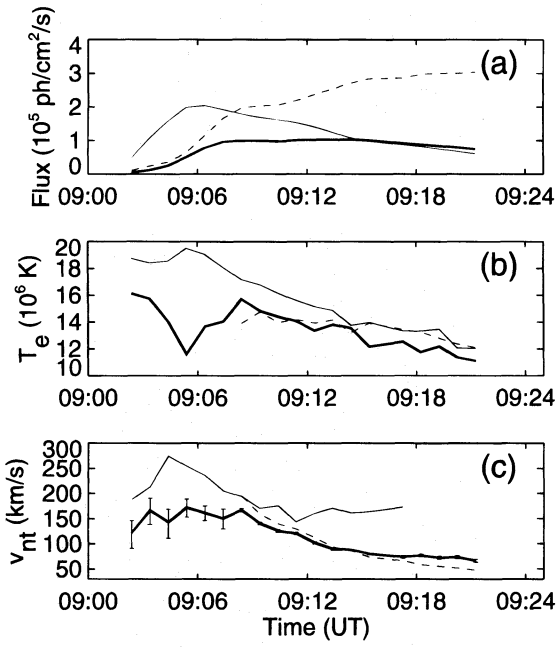

FIG. 2.—(*a*) BCS-derived fluxes, (*b*) electron temperatures, and (*c*) nonthermal velocities as functions of time during the 1993 April 15 flare for Fe XXV (*thin solid lines*), Ca XIX (*thick solid lines*), and S XV (*dashed lines*). S XV fluxes in (*a*) are reduced by a factor of 3. Results for the primary component are shown for Fe XXV and Ca XIX in (*b*) and (*c*) when two-component fits are used between 09:02 and 09:08 UT. Results for S XV at early times are unavailable for these two panels due to lack of coverage on the short-wavelength side of the resonance line. Error bars in (*c*) are from minimized χ^2 goodness of fit for Ca XIX.

component for Fe XXV and Ca XIX, and we omit early-time S XV v_{nt} values since we do not have two-component fits for those spectra. By nonthermal velocity, we are referring to the quantity associated with the width of the spectral lines in excess of that expected from T_e defined by

$$v_{nt} = [2k(T_D - T_e)/m_i]^{1/2} , \quad (2)$$

where T_D is the Doppler temperature corresponding to the symmetric width of the spectral line, k is Boltzmann's constant, and m_i is the mass of the Fe XXV, Ca XIX, or S XV ion.

Figures 3, 4, and 5 show spectra at three different times during the rise phase: 09:02:24, 09:03:24, and 09:06:24 UT (thick lines), respectively. These are all overlain onto spectra at 09:17:15 UT (thin lines), which is much later in the flare's development. Fe XXV, Ca XIX, and S XV spectra are in panels (*a*), (*b*), and (*c*), respectively. For Fe XXV we limit the display to the wavelength region in the neighborhood of the resonance line, while for the Ca XIX and S XV channels we show the entire observed wavelength ranges. Each panel has normalized intensities between the early- and late-time spectra so that the heights of the peaks of the resonance lines are identical, with the vertical axes labeled for the early-time spectra fluxes. In each case, the spectra are integrated for 60 s. Over the three early times, the location in wavelength of the spectra for each channel displays significant variations. At later times (after ≈9:12 UT), we do not see such variations in wavelength of the lines, as is demonstrated in Figure 6 discussed below. Therefore, we regard the 09:17:15 spectrum as representative of spectra of the flare after wavelength variations due to various motions

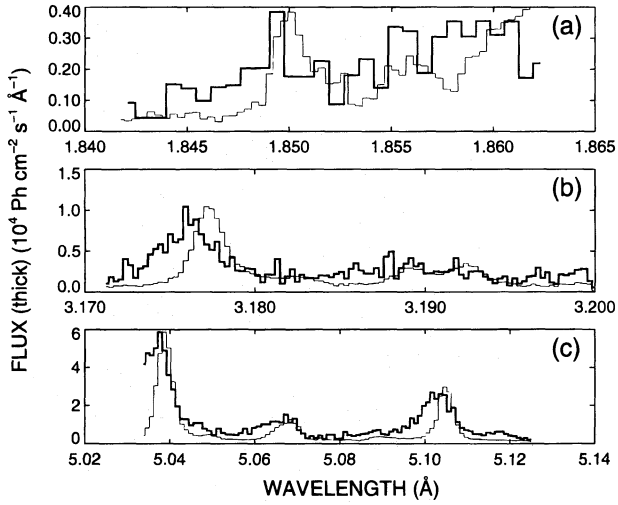

FIG. 3.—Spectra from 09:02:24 UT (*thick lines*) overlain onto spectra from late in the flare at 09:17:15 UT (*thin lines*) for (*a*) Fe XXV, (*b*) Ca XIX, and (*c*) S XV. Fluxes listed on the vertical axis are for the early-phase spectra, and the fluxes of the late-phase spectra are normalized so that the heights of the resonance lines are identical in the early- and late-phase spectra. The early-phase Fe XXV spectrum is double binned. The early-phase spectra are blueshifted relative to the late-phase spectra.

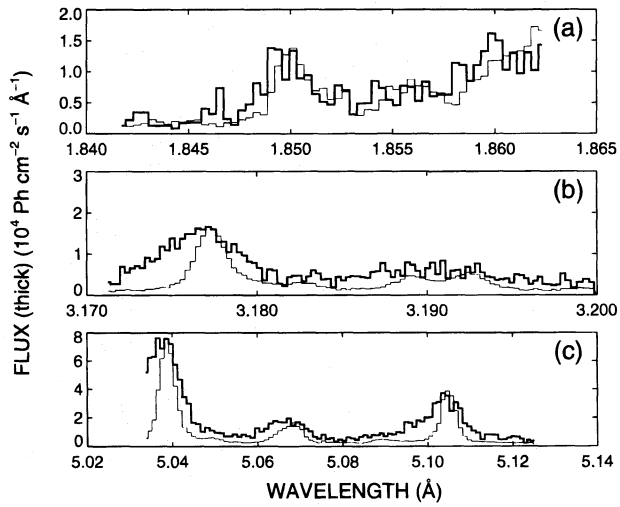

FIG. 4.—Same as Fig. 3, except the early-phase spectra (*thick lines*) are at 09:03:24 UT. The early-phase spectra are still strongly blueshifted.

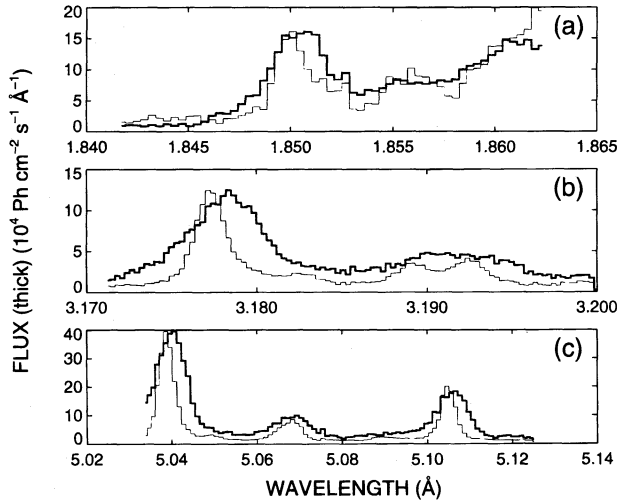

FIG. 5.—Same as Fig. 2, except the early-phase spectra (*thick lines*) are at 09:06:24 UT. The early-phase spectra are now strongly redshifted.

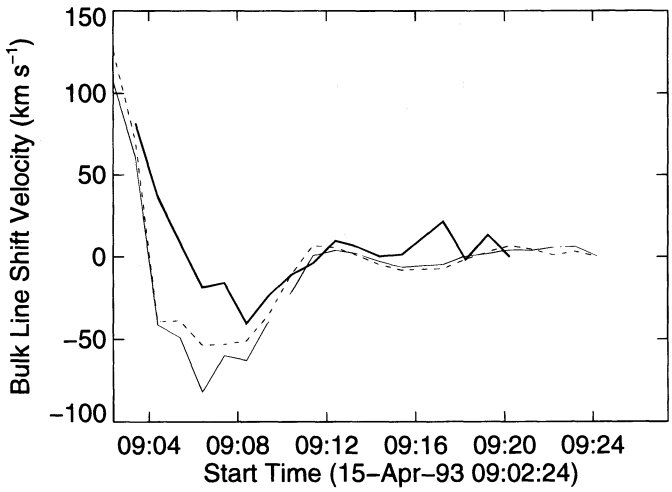

FIG. 6.—Centroid of the resonance lines of Fe XXV (*thick solid line*), Ca XIX (*thin solid line*), and S XV (*dashed line*) as functions of time in the 1993 April 15 flare. Wavelength shifts have been converted to velocities assuming that the line shifts are caused by Doppler motions. Negative and positive represent red- and blueshifts, respectively. Velocities are set to zero late in the event, consistent with the plasma coming to rest during the flare's peak and early decay phase.

have subsided; that is, we take it to be a spectrum from plasma at rest in the flare with respect to the Earth.

In the early-time spectra in Figure 3, Ca XIX and S XV display pronounced bulk blueshifts compared to the later spectra. This seems to be true for Fe XXV also, but this is not easily verified due to the low statistics of the spectrum. (We have "double binned" the Fig. 3 Fe XXV early spectrum in order to increase the number of counts per bin.) In Figure 4, in which the early spectra are a minute later than in Figure 3, all three ions show strong blue components. There is a hint of a double-component structure in the Fe XXV spectrum: one component whose peak overlays that of the late-time spectrum, and another with a peak at substantially shorter wavelengths. Three minutes later, as shown in Figure 5, the spectra all show strong redshifts, with Ca XIX and S XV resonance lines completely shifted toward the red. Fe XXV shows a strong centroid shift toward the red, with a substantial component near the rest position of the resonance line of the 09:17:15 spectrum.

Figure 6 displays the variation of the centroid of the resonance line position as a function of time for the three ions. Thick solid, thin solid, and dashed lines represent the centroid locations of the Fe XXV, Ca XIX, and S XV resonance peaks, respectively. For each ion, we have converted the wavelength shifts into velocities, with the velocity at late times set to be zero, consistent with the line-producing plasmas being at rest with respect to Earth at late times. (We ignore recession motion of the source due to solar rotation, which is only about 2 km s^{-1} for the source location of AR 7469 discussed in § 2.) Negative and positive values represent red- and blueshifts, respectively. In producing this diagram, we have fitted all three ions with single-component spectra at all times. Thus, at early times we are following the position of the centroid of the resonance line averaged over primary and secondary components. Figure 6 reaffirms and expands upon what we observe in Figures 3, 4, and 5: Early on we see strong bulk line shifts toward short wavelengths, which change rapidly to bulk redshifts lasting from about 09:04 UT until about 09:12 UT, with little motion of the resonance line position at later times.

In addition to bulk spectral line shifts, at the same time, early calcium and iron spectra also display blue wings. Figure 7 shows an example of two-component fits to the 09:04:24 Fe XXV (Fig. 7*a*) and Ca XIX (Fig. 7*b*) spectra. In each case, the histograms represent the observed spectra, thin solid and dashed lines represent the primary and secondary component fits, respectively, to the observed spectra, and the thick solid line is the sum of the two separate components. Relative velocities between the primary and secondary components are 350 and 225 km s^{-1} for Fe XXV and Ca XIX, respectively. Table 1 gives a summary of two-component fits for Fe XXV and Ca XIX, showing the relative velocities of the two components and the ratios of the emission measures of the secondary to the primary components at each time. As discussed in § 2, S XV spectra during the same time frame may also have strong blue wing asymmetries, but their magnitudes are hard to determine due to lack of coverage on the short-wavelength side of the S XV resonance line.

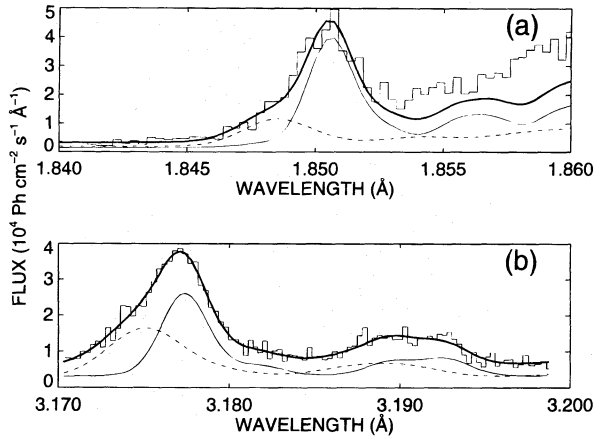

FIG. 7.—Two-component fits to early phase (*a*) Fe XXV and (*b*) Ca XIX spectra at 09:04:24. Dashed and thin solid lines represent the secondary and primary components, respectively, the thick solid line represents the sum of the two components, and the histograms are the observed spectra.

4. SOFT X-RAY IMAGES

Figure 8 shows a mosaic of 39 × 39 pixel (=96″ × 96″) portions of partial frame images from SXT obtained with the Be filter, covering selected times between 09:06:19 and 09:15:53 UT. Intensities are normalized over the entire set of images, so that brightness variations from frame to frame are indicative of real intensity changes. We will do a quantitative study of the images below. West is to the right and north is up in each panel, and the approximate position of the solar limb is overlain in each panel.

These images lack the clearly defined loop structures seen in many SXT flare images (e.g., Tsuneta et al. 1992; Doschek et al. 1995). This may be because we are observing above the primary flaring X-ray loops, if they are obscured by the limb. Another possibility is that we are viewing loops edge-on, as discussed in § 5, so that the loop shape is not obvious.

TABLE 1

TWO-COMPONENT FIT RESULTS FOR FE XXV AND CA XIX

Time	Fe XXV Velocity[a] (km s^{-1})	Fe XXV EM(s)/EM(p)[b]	Ca XIX Velocity[a] (km s^{-1})	Ca XIX EM(s)/EM(p)[b]
09:02:24.....	...	...	140	0.71
09:03:24.....	...	...	260	0.63
09:04:24.....	350	0.40	225	0.90
09:05:24.....	400	0.20	240	0.65
09:06:24.....	400	0.25	210	0.87
09:07:24.....	350	0.10	230	0.27

[a] Difference in velocities between primary and secondary components.
[b] Ratios of emission measures of secondary to primary components.

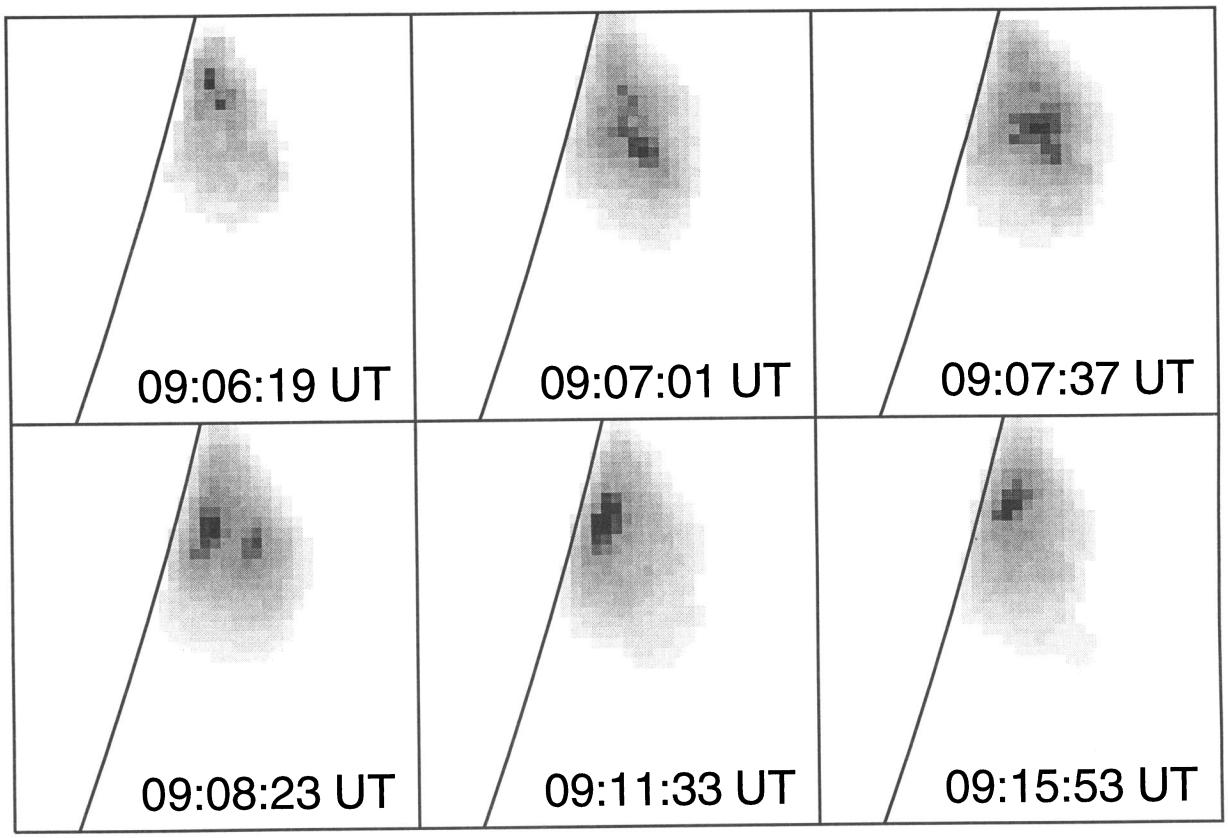

FIG. 8.—A mosaic of 39 × 39 pixel (=96″ × 96″) subframes of SXT partial frame images obtained with the Be filter at selected times. North is up, west is to the right, and the solar limb is overlain on each frame. Intensities are normalized over the entire set of images, so that brightness variations from frame to frame are indicative of real intensity changes.

Some intensity variations are visible in the images, with two regions of intensity enhancements visible in some frames. This is clearest in the 09:08:23 image, with one brightening near the limb and the other extended away from the limb. At later times, extensions move out toward the southwest in the image, as shown in the 09:15:53 UT frame.

Figure 9 shows an SXT Be filter image of the flaring region at 09:08:23 overlaid with contours. Boxes E and W denote east and west regions, which are respectively near to and separated from the limb. The box labeled "Total" denotes the entire region. Movies constructed from the partial frame images suggest that the intensity enhancement of region W may develop out of flows from region E between 09:07:01 and 09:08:23 UT. After this time, the emission gradually becomes more concentrated along the limb (region E).

Figure 10*a* shows the intensity variations of each region marked in Figure 9 as functions of time, with the dashed, thick solid, and thin solid lines representing regions E, W, and Total, respectively. For comparison, in Figure 10*b* we plot the Ca XIX intensity (from Fig. 2*a*) as the dashed line and Ca XIX bulk line shift (from Fig. 6) as the solid line. While region E shows a roughly constant increase in intensity with time, region W's intensity starts low, rises to a peak at about 09:07 UT, and then decreases slowly until after 09:10 UT. This intensity variation of region W coincides closely with the redshifts shown in Figure 10b, which peak near 09:06 and end near 09:11 UT. In contrast, region E's intensity does not show any correlation in time with the variations in spectral lineshifts. These results suggest that the region W feature is responsible for the strongest spectral redshifts in this flare. Also, the intensity extensions to the southwest visible in the 09:15:53 frame of Figure 8 occur at times at which there are no strong BCS spectral line shifts, so the extensions must not be related to the line shifts. Since partial frame SXT images are not available prior to 09:06:19 UT, we are unable to correlate images with the strong BCS blue line shifts or the initial buildup of the strong redshifts.

North-south displacements in SXT correspond to a velocity of 1.11 km s^{-1} $arcsec^{-1}$ in the BCS Ca XIX channel (Mariska 1994). Figures 8 and 9 indicate that the north-south extent of the flare in the Be filter is of order 30″ at all times when the line shifts are large, corresponding to an equivalent spectral shift of about 35 km s^{-1} in the BCS Ca XIX channel. This is considerably less than the values in Table 1, and therefore it indicates that the line shifts are caused by Doppler motions rather than north-south movement of source position or the north-south extent of the source.

Broadening of the spectral lines due to this north-south extent provides a negligible contribution to the non-thermal velocity of the observed spectrum (see Fig. 2*c*) during times of SXT partial frame images. For example, at 09:14:53 UT, removing source-extent contribution from the nonthermal broadening of the full observed spectrum ($\approx$80 km s^{-1}; see Fig. 2*c*) leaves a flare spectrum with a nonthermal line broadening corresponding to a velocity of about 70 km s^{-1} (assuming Maxwellian distributions for the components of

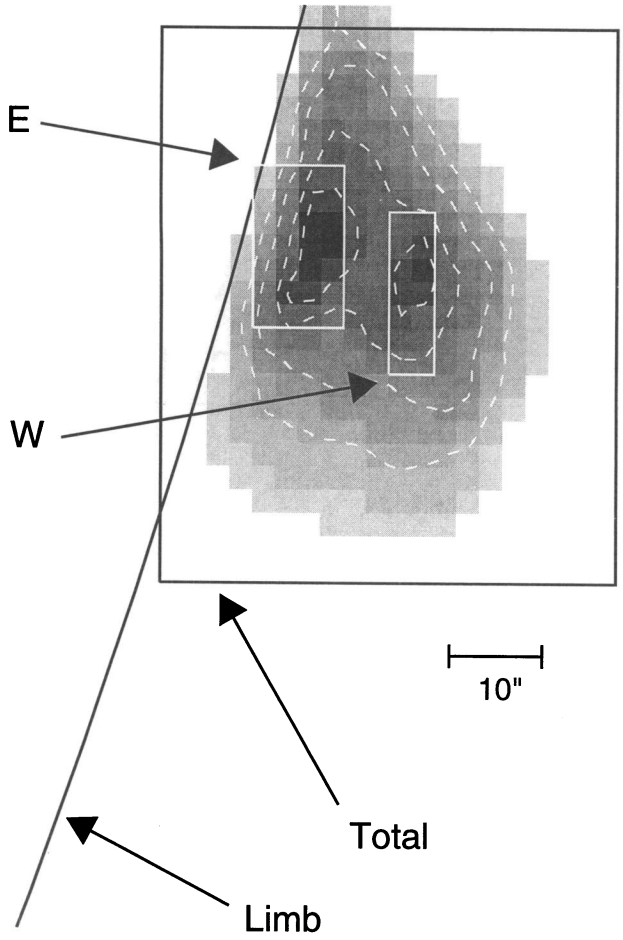

FIG. 9.—SXT partial frame image at 09:08:23 UT (cf. Fig. 8). Region E marks a bright feature near the limb, region W marks a feature suspended away from the limb, and "Total" marks the entire flaring region. Intensities of these regions are shown in Fig. 10*a*. Contours are at 40%, 60%, 80%, and 90% of the peak intensity.

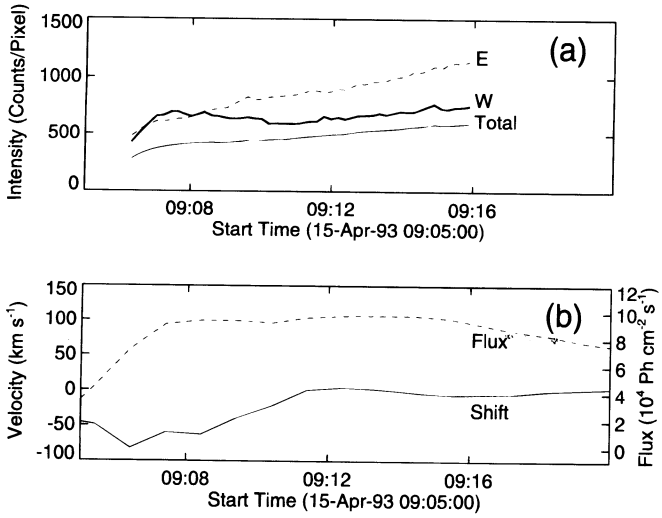

FIG. 10.—Spatially averaged intensities from the SXT Be filter of regions E (*dashed line*) W (*thick solid line*), and Total (*thin solid line*) marked in Fig. 9 as functions of time during the flare. (*b*) Intensity (*dashed line;* see Fig. 2*a*) and Doppler velocity of the centroid (*solid line;* see Fig. 6) of Ca XIX. Intensity variations in region W of Fig. 9 coincided closely with bulk redshifts in Ca XIX.

the line broadening). This means that the spatial distribution of the flaring source accounts for only $\lesssim 10\%$ of the observed Ca XIX nonthermal broadening near time of peak intensity of this flare.

5. DISCUSSION

Using spectral data from BCS and images from SXT, we have found strong bulk and blue wing spectral line shifts in the upper atmosphere of a flare occurring well beyond the solar limb. Most of the strong bulk redshifts appear to emanate from region W in the SXT image of Figure 9. Due to lack of coverage of SXT partial frame images, we are unable to determine the source of the bulk line shifts prior to 09:06:19 UT.

Over-the-limb flares are sometimes detectable in hard X-rays (e.g., Frost & Dennis 1971; Hudson 1978; Kane et al. 1992). This event, however, is not prominent in *Yohkoh*'s hard X-ray telescope (HXT), which shows a weak, featureless event wth a duration of about 5 minutes in its 14–23 keV channel. A weak excess (of marginal significance) also appears to be present in the HXT 23–33 keV channel after about 09:06 UT (when observations in that channel commence). From the ratio of counts in these two channels, we find a temperature of $19.3–23.0 \times 10^6$ K. No signal is discernible in higher HXT channels, and overall the hard X-ray fluxes are too low for successful HXT imaging. Due to the steepness of the hard X-ray spectrum, we would not expect an extended nonthermal event to be present, and indeed no type II or type IV emission is listed in the NOAA *Solar-Geophysical Data* for the time of this flare.

Images from both *Skylab* and SXT indicate that the strongest soft X-ray emission from flares is often localized to one primary loop (Acton et al. 1992). Such loops are generally smaller than the loops that we see for this flare, which are probably much larger than 50,000 km, as determined in § 2. Therefore, unless we are observing a particularly large loop-size event, our work here indicates that there are structures beyond the primary flaring loop generally seen in soft X-ray images. Such structures may normally be overwhelmed in brightness by the lower loops. In order to attempt to interpret our observations, we will assume that we are effectively observing a single loop (i.e., either a single loop or an arcade of loops oriented in the same direction) and perhaps sitting above one or more lower lying and brighter loops which are occulted by the solar disk. Let us assume further that strong upflows, consistent with evaporation flare models, occur on this large, effectively single loop. We will consider cases in which these upflows (i) are symmetric from both loop footpoints and terminate near the loop apex, and (ii) are one-sided, emanating from one footpoint only.

If the loop is oriented "face-on" relative to the Earth, as shown schematically in Figure 11*a*, then the symmetric upflows along the loop would produce redshifts in BCS, since the over-the-limb loop would be inclined away from the Earth. These redshifts could be ≈ 80 km s^{-1} if the upflows along the loop are 200 km s^{-1}, assuming source location as determined in § 2. Although this is similar to the velocities of the redshifts that we observe (Fig. 6), this scenario cannot account for the blue wings which we observe simultaneously with the redshifts. If the upflows are one-sided rather than symmetric, then we would expect to see a progression of BCS spectral line shifts going from red to more or less "stationary" as plasma passes the apex of the

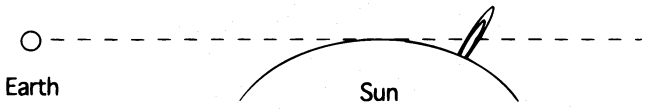

FIG. 11*a*

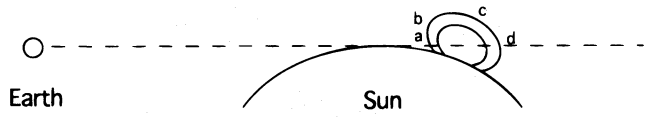

FIG. 11*b*

FIG. 11.—Schematic diagram of the orientation of the flaring loop with respect to Earth. (*a*) Loop "face-on" with respect to Earth. (*b*) Loop "edge-on" with respect to Earth. In the edge-on case, more of the loop leg furthest from Earth is obscured than the loop leg nearest Earth. Labels "a," "b," "c," and "d" refer to the location on the near leg which intersects the line of sight from Earth, where the Earthward component of upflows on the near leg changes sign, the loop apex, and where the far leg intersects the line of sight from Earth, respectively. There may be one or more brighter flaring loop(s) residing beneath the single loop drawn in the schematic.

loop. This is because the upgoing redshifted and downflowing blueshifted effects would tend to cancel each other out when flows are on both sides of the loop apex. This scenario predicts that the largest redshifts would occur when the brightest material is moving up the lower or middle part of the upflow leg of the loop. That is, the largest redshifts would occur several minutes prior to the time at which plasma producing the brightest emission measure reaches the loop apex, assuming velocities of 200 km s^{-1} and a loop half-length of 50,000 km. But Figure 10 indicates that the time of peak redshifts and the time of peak SXT flux near the top of the loop are simultaneous to within about 1 minute. Therefore, we do not believe that this one-sided flow, face-on scenario is likely. There is also no ready explanation in the face-on picture (with either symmetric or one-sided upflows) for the bulk blueshifts we observe at early times.

Next we consider that the loop is oriented "edge-on" to Earth, as shown schematically in Figure 11*b*. In this case, one leg of the loop (the "near leg") will be closer to Earth than the other (the "far leg"). Label "a" refers to the location at which the near leg intersects the line of sight from Earth, "b" is where the Earthward component of upflows on the near-leg changes sign, "c" is the loop apex, and "d" is where the far leg intersects the line of sight from Earth. If flows are symmetric, then flows along segments a-b and c-d will appear blueshifted, and flows along segment b-c will appear redshifted. Depending on the actual geometry of the loop and the "degree of symmetry" of the upflows, emission measure of the redshifted segment may be greater than the sum of the emission measures from the two blueshifted segments. In that case, we would expect red and blue components to coexist in BCS spectra, with the red component dominating the blue component because of its larger emission measure. This is just what we see in the April 15 flare between $t \approx 09{:}04$ and 09:08 UT; that is, we observe bulk redshifts augmented by a smaller emisson measure blue wing at those times. If the upflows are one-sided and initiate from the near leg's chromosphere, then flows along the b-c-d segment will be redshifted, and flows along the a-b segment will be blueshifted. This could also explain our spectral observations of predominant redshifts augmented by a smaller blueshifted emission measure. In both the symmetric and one-sided upflow cases, the bulk blueshifts we observe prior to $t = 09{:}04$ UT could be explained by upflows along the a-b segment of the edge-on loop at early times before much of the plasma enters the b-c segment of the loop. These earliest upflows would have relatively high velocities and low emisson measure compared to later upflows (consistent with Fig. 6), since they would be caused by material ablated off of the uppermost region of the chromosphere. Our assumption that the loop segment a-b is inclined toward Earth seems to be necessary in order to explain these early-time bulk blueshifts. Given this, the orientation shown in Figure 11*b* can explain all key aspects of the spectral line shifts that we observe, subject to specifics of the loop geometry which are indeterminable from our data. Moreover, the geometry of the loop between the solar surface and location "a" on the near leg, and between the solar surface and location "d" on the far leg, is not important since those regions are not visible from Earth. Thus, the loop is not necessarily symmetric as in the Figure 11 sketch.

This "edge-on" loop interpretation is also consistent with the SXT images, which indicate that material may be flowing upward from the base toward the apex of the loop, and that the redshifts seem to emanate from the bright material separated farthest from the limb as seen from Earth. Since this chance alignment would not be expected to occur so frequently, we have a natural explanation for why strong line shifts are not common in limb and near-limb flares. Morphologically, this event may be similar to the 1992 February 17 flare discussed by Doschek et al. (1995), but seen edge-on and over the limb instead of on the solar disk.

By appealing to more complicated geometries for the flaring structures, we could construct different circumstances consistent with our observations. For example, two loops, one oriented as in Figure 11*a* and the other oriented as in Figure 11*b* with respect to Earth, could presumably explain our observations given appropriate flow velocities in each loop. Nothing in the SXT images, however, suggests this type of geometry. Also, it is difficult to rule out the possibility that the BCS spectral line shifts result from one or more flaring loops oscillating in the line of sight with Earth. We do not take up these more complex possibilities here.

We find that there are substantial nonthermal velocities present in the spectra, even though our observations are restricted to the uppermost portions of the flare. These velocities for Ca XIX, near 150 km s^{-1} during the rise phase (for the primary component) and dropping to around 60 km s^{-1} at later times, are comparable to the nonthermal velocity magnitudes and behavior with time seen in disk flares in previous studies (e.g., Doschek 1990). That is, the quantities are similar if we observe high in the upper portions of the soft X-ray flare, as we do here, or if we observe flares on the disk for which the footpoints are also visible. These findings are similar to those regarding nonthermal velocities for over-the-limb flares of Khan et al. (1995) and Mariska et al. (1996), in that those two studies also found enhanced nonthermal velocities in footpoint-occulted flares. (Mariska et al., comparing directly *Yohkoh* observations of footpoint-occulted flares and disk flares, found the nonthermal velocities to be somewhat higher in the disk flares. Khan et al.

citing only previous non-*Yohkoh* results for disk flares, found comparable values for both.) Our observations of nonthermal velocities are at even higher heights in the flare corona than those of the Khan et al. and Mariska et al. studies.

If we are indeed looking at flaring loops oriented edge-on to Earth, as in Figure 11*b*, then there is the possibility that the enhanced line broadening is caused by a superposition of directed material flows along the loop toward and away from Earth. With Figure 7, we are assuming that any such directed flows separate out into two spectral components. But each of these two components is broadened beyond thermal values. One possibility is that this broadening of the separate components represents a spread in velocities of material flowing on the loop. In that case, the line broadenings we see at these high altitudes may be essentially a coincidence of the loop orientation. Another possibility, however, is that much of the nonthermal broadening we see results from some mechanism other than a distribution of plasma flows, such as plasma turbulence, or as a consequence of reconnection above the primary soft X-ray loops (see Tsuneta 1995). Our work here does not allow us to differentiate between these two possibilities.

We find that near time of peak flare intensity in Ca XIX, $\lesssim 10\%$ of the nonthermal velocities may be explainable by an extended source such as that seen in the SXT images. Watanabe (1990) found that the finite distribution of the source may be a major contributor to the decay-phase Fe XXV nonthermal velocity signature in a flare observed by *Hinotori*. We do not have SXT images during the later decay phase for this event, so we are unable to compare our findings with the Watanabe results here.

We thank K. Akita, J. L. Culhane, J. A. Klimchuk, and K. T. Strong for valuable scientific discussions, and G. A. Linford and D. M. Zarro for software assistance. A. C. S. acknowledges support from NRL/ONR basic research programs. H. S. H. and J. R. L. acknowledge support from NASA contract NAS 8-37334. A portion of this work was carried out while L. K. H.-M. was at the School of Physics and Space Research, University of Birmingham, UK.

REFERENCES

Acton, L. W., et al. 1992, PASJ, 44, L71
Arnaud, M., & Raymond, J. 1992, ApJ, 398, 394
Arnaud, M., & Rothenflug, R. 1985, A&AS, 60, 425
Bely-Dubau, F., Dubau, J., Faucher, P., & Gabriel, A. H. 1982a, MNRAS, 198, 239
Bely-Dubau, F., et al. 1982b, MNRAS, 201, 1155
Culhane, J. L., et al. 1991, Sol. Phys., 136, 89
———. 1994, Sol. Phys., 153, 307
Doschek, G. A. 1990, ApJS, 73, 117
Doschek, G. A., et al. 1992, PASJ, 44, L95
———. 1994, ApJ, 431, 888
Doschek, G. A., Strong, K. T., & Tsuneta, S. 1995, ApJ, 440, 370
Emslie, A. G., Li, P., & Mariska, J. T. 1992, ApJ, 399, 714
Feldman, U., Hiei, E., Phillips, K. J. H., Brown, C. M., & Lang, J. 1994, ApJ, 421, 843
Fludra, A., Lemen, J. R., Jakimiec, J., Bentley, R. D., & Sylwester, J. 1989, ApJ, 344, 991
Frost, K. J., & Dennis, B. R. 1971, ApJ, 165, 655
Harra-Murnion, L. K., et al. 1996, A&A, in press
Howard, R. D., Harvey, J. W., & Forgach, S. 1990, Sol. Phys., 130, 295
Hudson, H. S. 1978, ApJ, 224, 235
Kane, S. R., McTiernan, J., Loran, J., Fenimore, E. E., Klebesadel, R. W., & Laros, J. G. 1992, ApJ, 390, 687
Khan, J. I., Harra-Murnion, L., Hudson, H. S., Lemen, J. R., & Sterling, A. C. 1995, ApJ, 452, L153
Lang, J., et al. 1992, PASJ, 44, L55
Mariska, J. T. 1994, ApJ, 434, 756
Mariska, J. T., Emslie, A. G., & Li, P. 1989, ApJ, 341, 1067
Mariska, J. T., Sakao, T., & Bentley, R. D. 1996, ApJ, 459, 815
Nagai, F., & Emslie, A. G. 1984, ApJ, 279, 896
Newton, E. K., Emslie, A. G., & Mariska, J. T. 1996, 459, 804
Sterling, A. C., Doschek, G. A., & Pike, C. D. 1994, ApJ, 435, 898
Tsuneta, S. 1995, PASJ, 47, 691
Tsuneta, S., et al. 1991, Sol. Phys., 136, 37
Tsuneta, S., Hara, H., Shimizu, T., Acton, L. W., Strong, K. T., Hudson, H. S., & Ogawara, Y. 1992, PASJ, 44, L63
Watanabe, T. 1990, Sol. Phys., 126, 351